https://dx.doi.org/10.1016/j.jcsr.2022.107454

Flexural behaviour of cold-formed steel square and rectangular hollow sections with moderate heat-treatment

Paola PANNUZZO and Tak-Ming CHAN*

Department of Civil and Environmental Engineering,

The Hong Kong Polytechnic University, Kowloon, Hong Kong SAR, China

**tak-ming.chan@polyu.edu.hk*

Abstract

This paper discusses the flexural behaviour of cold-formed square and rectangular hollow steel sections (SHSs and RHSs) with subsequent heat-treatment through experimental and numerical investigations. Firstly, an experimental programme comprising tensile coupon tests on flat and corner regions and three-point bending beam tests were conducted. A total of 12 specimens were tested under monotonic bending loads, covering a variety of section slenderness. Failure modes, moment-rotation curves and plastic hinge lengths have been evaluated highlighting the effect of the web-flange interaction on rotation capacity. Successively, experimental results were combined with numerical FE results to assess the corresponding moment and deformation capacities. Current cross-section classification limits given in Eurocode 3 and AISC 360-16 were assessed and new limits has been proposed.

Keywords

Structural hollow section; cold-forming with heat-treatment; bending tests; Finite Element modelling; cross-section classification.

1. Introduction

Structural hollow sections are widely used in engineering applications owing to their structural efficiency, in particular for their high strength-to-weight ratio and high torsional stiffness. Their structural behaviour mainly depends on the manufacturing processes which may lead to significant differences in mechanical properties. Broadly speaking, structural hollow sections can be classified into two major groups: Cold-Formed and Hot-Finished. Both groups are made from hot-rolled steel plates which are roll-pressed at very high temperatures, over 850°C, and then, cooled at room temperature. This hot-rolled steel plates result in normalized condition (free from internal stresses). By cold-forming process, hot-rolled steel plates can be bent and welded into square or rectangular hollow sections. These sections are part of the "Cold-Formed" group, in accordance with EN-10219-1,2 [1,2].

Due to the bending process, cold-formed sections present enhanced strengths at the corners, which reduce ductility and present points of weakness in the sections along which cracks might form. In addition, the bending process together with the welding procedure creates internal stresses across and along the hollow sections. Nevertheless, by subsequent heat treatment, it is possible to relieve these stresses and improve ductility. These sections are referred to "Hot-Finished" group in accordance with EN 10210-1,2 [3,4]. Specifically, within EN 10210-1, two types of sections can be produced: "hot-finished" and "fully normalized". The so-called "hot-finished" sections refer to cold-formed hollow sections with moderate heat treatment; whereas, "fully normalized" sections refer to cold-formed hollow sections subsequently heat-treated at approximately 850°C. Therefore, "fully normalized" sections present the same properties of the virgin hot-rolled steel plates and can be considered as equivalent Hot-Formed sections.

However, specific requirements regarding the temperature and holding time of "hot-finished" process seem to not be present in the standard and the steel manufacturing process shall be at

the discretion of the steel producers. Therefore, under the name of “hot-finished”, hollow sections may have different mechanical properties.

In the last decades, experimental and numerical investigations were carried out on different types of hollow sections to assess their load-carrying capacities, highlighting the differences in terms of material properties, geometric imperfections, residual stresses, corner geometry and structural performance [6-13].

Zhang et al. [5], compared hot-formed, cold-formed and hot-finished hollow sections under monotonic loading at material level and confirmed that cold-formed hollow sections show higher strengths but the ductility in terms of elongation and tensile ratio is much worse compared to hot-formed sections. Moreover, the ductility of hot-finished sections is not the same as hot-formed sections, although they are treated equally in EN 10210 [3,4].

Nonetheless, there is still a lack of understanding of structural behaviour of hot-finished members, or better, the structural behaviour of cold-formed steel hollow sections with moderate heat treatment that needs to be furtherly investigated.
In other words, the issue related to the so called ‘hot-finished’ sections is to understand if they behave more like hot-formed sections as they follow the same standard or if they behave as cold-formed sections with an improvement in ductility owing to the final heat-treatment.

Indeed, hollow steel sections still represent an alternative for bending applications, as they are not susceptible to lateral torsional buckling. The development of adequate ductility or deformation capacity is a fundamental condition for bending applications. Hence, the main purpose of this research is to investigate the flexural performance of cold-formed sections with moderate heat-treatment, in particular, to evaluate the contribution of heat-treatment on rotation capacity of beam members and their applicability within the current design standards.

Nowadays, in Eurocode 3 [14] and North American code AISC 360-16 [15], the rotation capacity of member is considered through the cross-section classification. This is based on the limits of width-thickness, *b/t*, and depth-thickness, *d/t*, ratios of the cross-section.

It is required that members, to be used in plastic design, shall achieve rotation capacity *R* equal or more than 3 before the onset of local buckling. Eq. (1) defines the rotation capacity *R* [16].

$$R = \frac{\Theta_{\mathrm{u}} - \Theta_{\mathrm{y}}}{\Theta_{\mathrm{y}}} \quad (1)$$

where Θ_u is the ultimate rotation and Θ_{y} is the yielding rotation as shown in the generalized moment-rotation curve of a ductile steel member, Fig. 1.

In this research, both experimental and numerical investigations have been carried out and are presented in the following sections.

2. Experimental Programme

2.1 General

A comprehensive testing programme on S355J2H steel square and rectangular hollow sections (SHSs and RHSs, respectively) manufactured according to EN 10210-1 [3]was conducted under flexural loading. Note that, as previously mentioned, “hot-finished” sections refer to cold-formed sections with moderate heat-treatment. 10 section sizes were chosen to provide an appropriate range of width-to-thickness (*b/t*) and depth-to-thickness (*d/t*) values within plastic design. Square Hollow Section (SHS) and Rectangular Hollow Section (RHS) with geometric symbols are presented in Fig. 2. Measured section properties are listed in Table 1.

Regarding the cross-section classification of hollow sections, no distinctions are made for hot-finished or cold formed section in Eurocode 3; whereas, cross-section limits in AISC360-16 are specifically related to the cold-formed hollow structural sections.

95 Firstly, the specimens have been classified based on the steel nominal yield strength and the
96 current local slenderness limits in respective codes, as shown in Table 1 and Fig. 3. As it can
97 be noted, although different terminologies are employed in the two codes, the basic design
98 principles and their limits are similar. Sections classified as class 1 or Compact are suitable for
99 plastic design.

100 Furthermore, 2 out of 10 sections were tested with different lengths in order to provide more
101 information about the influence of member slenderness on flexural performance.

102 Therefore, a total of 12 hollow steel sections were tested in bending under monotonic loading.
103 Each specimen was prepared with a specimen label, starting with the initials "SHS" or "RHS"
104 to identify it as Square or Rectangular Hollow Sections, respectively; followed by the nominal
105 section size, then, letters "ST" or "SL" to indicate STocky or SLender members, respectively,
106 in case same sections having two different lengths.

107 **2.2 Material Tensile Tests**

108 To determine the material properties, three flat coupons were extracted from each cross section
109 and two corner coupons from three typical sections with different tube thicknesses - SHS-
110 100×100×8, SHS-120×120×6.3 and SHS-100×100×4, in accordance with BS EN ISO 6892-
111 1:2016 [17]. All coupons were tested in Instron 8803 Fatigue Testing System with capacity of
112 500 kN. Typical measured stress-strain curves are plotted in Fig. 4, showing the SHS
113 100×100×4 coupon results. Flat coupons display the anticipated sharply defined yield point,
114 yield plateau, and subsequent strain hardening, as expected for hot-rolled steel, whereas the
115 corner coupons present less strain hardening as typical of cold-formed sections.

116 The average material characteristics are listed in Table 2, including yield strength (f_y), elastic
117 modulus (E_s), yield strain (ε_y), strain when strength hardening initiates (ε_{sh}), ultimate tensile

strength (f_u), strain corresponding to the ultimate tensile strength (ε_u), elongation after fracture based on the original gauge length (ε_f) and the hardening ratio (f_u/f_y).

Eurocode 3 requires a minimum ductility expressed in terms of limits $f_u/f_y \geq 1.10$, elongation at failure not less than 15% and $\varepsilon_u \geq 15\varepsilon_y$. As it can been observed from Table 2, flat coupons largely meet all these requirements, whereas, corner coupons hardly achieve the requirements due to the effects of cold working. However, these cold-formed steel sections with moderate heat-treatment may show satisfactory steel ductility as the flat region covers the main part of the cross-section.

2.3 Test Setup and Instrumentation

Fig. 5 illustrates the reaction frame at the Structural Engineering Research Laboratory of The Hong Kong Polytechnic University which was designed and its applicability was proven for the experimental testing of three-point simply-supported beams previously carried out by Chen and Chan [18].

As shown in Fig. 6, the effective flexural length, L_f , was defined as the length measured from the end support to the edge of the rigid connector. The load was applied under displacement control through a rigid connector welded to the specimen at the mid-span. Greased steel rollers were used to achieve simple-support conditions.

For each specimen, four strain gauges were adhered to the tensile and compressive flanges, at a distance of 10 mm and 200 mm from the loading point. End rotations and mid-span deflections were recorded digitally throughout the tests by means of LVDTs.

A total of 8 LVTDs were used : LVDTs 1-2 are to measure the deflection at mid span and to make sure that the connector behaved as rigid body, LVDTs 3-4 are to measure the lateral

displacements at specific locations and LVDTs 5-8 are to measure the horizontal displacements, as presented.

3 Experimental Investigation

3.1 Failure modes

Fig. 7 shows the typical failure modes with outward bulging developed at the compressed plates at the midspan of the beams in correspondence of maximum strength (see Fig. 7a). By increasing the displacement level, the flange bulge deformation also increased involving the depth of the section (see Fig. 7b). Web-flange buckling interaction led to a severe drop of the flexural performance with a substantial reduction of rotation capacity. As expected, local buckling became more significant with the increase of local slenderness.

3.2 Rotation capacity

The local ductility, or rotation capacity, has been evaluated on the basis of moment-rotation (M- Θ) response of each specimen. The moment, M, was calculated as defined by Eq. (2) .

$$M = \frac{P \times L_f}{2} \quad (2)$$

where P is the applied load and L_f is the effective flexural length.

The rotation Θ, or drift ratio, is defined as the lateral displacement, δ, from LVDT 1, over the flexural length, see Eq. (3).

$$\Theta = \frac{\delta}{L_f} \quad (3)$$

To facilitate the comparison among different cases, normalized moment (M/M_{pl}) has been plotted against the rotation Θ, as presented in Fig. 8.

In general and as anticipated, it can be observed that higher are the width-to-thickness (b/t) and depth-to-thickness (d/t) values, higher is the plastic deformation capacity before failure. Very compact sections can achieve large deformation levels without moment degradation.

Moreover, increasing the local slenderness, the different behaviour among square and rectangular hollow sections is more obvious. Rectangular hollow sections attained lower rotation levels than those square counterparts with similar b/t ratio. This may be explained by the interaction between flange and web local buckling. In particular, comparing SHS-150×150×5 ($b/t = d/t = 28$) and RHS-250×150×6.3 ($b/t = 21$, $d/t = 37$), the first one performed better even though it is classified in class 2 (Eurocode 3) or as non-compact section (AISC classification). Whereas, RHS-250×150×6.3 barely achieved the plastic moment before a sudden drop, showing poor ductility.

Moreover, the difference in behaviour among specimens with same section but different length has been minimal, thus, member slenderness seems to be a minor influence on flexural performance.

Furthermore, the over-strength factor, $M_{max}/M_{pl,}$ reduced with the increase in the local slenderness. This can be explained because more compact sections present higher strain-hardening before the onset of local buckling. It is worth noting that, the plastic moment ($M_{pl}=f_y$ x W_{pl}) has been calculated using the experimental yield strength f_y measured from flat coupon tests for each section and the plastic section modulus, W_{pl} . Considering that the yield strength in corner regions is on average 1.15 times higher than flat part this leads to slightly underestimate the effective plastic moment.

Table 3 presents the test results in terms of moment and deformation capacities. Note that the ultimate moment was calculated as 'theoretical' failure point at 80% of maximum moment M_{max} and Θ_u is the corresponding rotation value.

In terms of rotation capacity, *R*, the most compact sections confirmed their highly stable plastic behaviour without dropping their moment capacity ($R \geq 7$).

The square specimen SHS-150×150×5, classified as Class 2 or Non-Compact, achieved the plastic moment resistance with rotation capacity R = 3.8, whereas the rectangular section RHS-250×150×6.3, still classified as class1/compact section achieved, a lower rotation capacity, R=1.6.

These experimental findings suggest it is imperative to review the limits of cross-section classification for plastic design for hollow sections accounting for web and flange slenderness interaction in plastic design. To ensure adequate rotation capacity , width-to-thickness, *b*/*t*, limits may be relaxed , whereas, depth-to-thickness, *d*/*t*, limits shall be tightened

Although experimental data are limited, they can be considered as a basis to evaluate and assess the rotation capacity *R* of the cold-formed hollow steel sections with moderate heat-treatment for plastic design. A more thorough review of these limits can be made increasing the number of cases by parametric studies as presented in Section 4.

3.3 Plastic hinge development

Fig. 9 shows the lateral load versus strain curves of typical specimens, i.e. SHS-100×100×6.3 (Fig. 9a), SHS-100×100×4-ST (Fig. 9b) and SHS-100×100×4-SL (Fig. 9c).

The red dashed line indicates the yield strain value ε_y of steel obtained from tensile coupon tests. It can be observed that, in general, strain readings are symmetrical and show a linear trend in elastic range. After yielding of the steel, the strains measured near the rigid connector (from SG1 to SG4) increased. This strain increasing is more obvious in specimens with higher cross-section slenderness due to local buckling. In SHS-100×100×4-ST and SHS-100×100×4-SL, the strains measured by SG1 and SG2 increased dramatically, indicating that local buckling occurred.

211 Strains measured by SG5, SG6, SG7, SG8 might provide some indication on the length of
212 plastic hinge. The strains just reached and moderately exceeded the yield strain indicating that
213 the plastic hinge developed beyond 200 mm (~2*d*).
214

215 **4. Numerical Investigation**

216 **4.1 Modelling Assumptions and Validation**

217 A numerical investigation was conducted to further expand the limited experimental data.
218 Finite element models were firstly developed to replicate the experimental response and
219 subsequently to generate parametric studies on evaluation of flexural behaviour and
220 deformation capacity of cold-formed hollow steel sections with moderate heat-treatment.

221 The commercial finite element (FE) analysis program ABAQUS [19] was used to generate the
222 numerical FE models.
223 To increase the computational efficiency, simplified half model was adopted once confirmed
224 the validity of modelling approach by comparing with the full model, as shown in Fig. 10 in
225 terms of moment-rotation response (Fig.10a) and failure modes (Fig.10b) .
226 Fixed boundary conditions with free longitudinal displacement and free rotation along the
227 transversal axis were applied to the end, in correspondence to the rollers, whereas, fixed
228 boundary conditions with free vertical displacement were applied in correspondence to the
229 loading point position.
230 The FE model was discretized by 4-node shell elements. The element was divided into three
231 mesh regions: (i) the core region, starting where the load is applied till 1.5 times the dimension
232 of the largest side of the section, with a mesh size equal to the thickness of sections; (ii) a
233 transition region and (iii) an end region with a wider mesh size to represent the zone which
234 remains elastic. Boundary conditions and mesh discretization of FE model are shown in Fig.11.

Regarding the material characteristics, non-homogeneous properties were observed from flat and corner coupons results, therefore, different properties at corner and flat regions were assigned in the FE models. The mean values of material properties from the previously discussed tensile coupon tests, see Table 2, were converted to true stress and strain values then input and applied to the flat- and corner- regions of the FEA models.

The initial geometric imperfection was considered for the FE models by carrying out elastic buckling analysis. The mode shapes are similar to those observed during the experimental tests were used to simulate the distribution of local imperfections.

Moreover, a sensitivity study was conducted to select the magnitudes of geometric imperfection and, in parallel, to define the corner region length, namely, the distance beyond corners also affected by the strength enhancement due to the cold-working.

Starting from the tolerance value prescribed by BS EN 10210-2 [4], *s*/100, (s is the cross-section width) three amplitudes (*s*/100, *s*/200, *s*/300) were considered in three different FE models: (i) a simplified model using only flat coupon results, (ii) a simplified model considering corner coupon results only at the corner regions equal to 3*t* (*t* is the cross-section thickness) and (iii) a simplified model considering corner coupon results the corner regions plus adjacent flat portions of a distance equal to 2*t* . This is because the cold-working effect on the corner regions extending beyond the corners is typical equal to 2*t*, according to the findings of previous experimental research of cold-formed tubes [12]. This sensitivity study may be useful for evaluating the effect of heat-treatment mitigation. Fig.12 presents the different assignment conditions of corner and flat material properties. Table 4 summaries the ratios of maximum moment between the experimental and finite element results, using different local imperfection amplitudes and different corner regions in 4 typical specimens. As can be seen, the difference among different cases is minimal and directly choosing the manufacturing tolerance (*s*/100) for imperfections and only tensile flat results for all sections might be on the

conservative side; however, this choice may anticipate the onset of local buckling and not correctly predict the effective plastic hinge formation observed during experimental testing. Therefore, the combination of "Only Corner Region" and the *s*/200 value, half of the tolerance, was adopted for all FE models to accurately capture the local buckling behaviour. Residual stresses were not explicitly incorporated into the FE models for two reasons: i) the main effect of residual stresses is the earlier initiation of the yielding process with no impact on the rotation capacity, 2) the longitudinal bending residual stresses are inherently counted within the stress-strain curves obtained from tensile coupon tests.

Fig.13 shows a typical comparison in terms of failure patterns. The shape and location of local buckling in the FE model (see Fig.13b) are highly consistent with those observed in the experimental test (see Fig.13 a).

The comparisons among the test and predicted moment-rotation curves of the 12 specimens are given in Fig. 14 and Fig. 15 for SHS and RHS respectively. A good agreement can be observed and, as stated above, the earlier initiation of the yielding process in the finite element results may be related to the fact that residual stresses were neglected: though, no impact on the deformation capacity was observed.

4.2 Parametric investigation

Following the successful validation of the FE models, based on the simplified model considering corner coupon results only at the corner regions equal to 3*t* (*t* is the cross-section thickness), a parametric study was carried out to assess the rotation capacity of cold-formed hollow steel beams with moderate heat-treatment.

A wide range of section sizes was considered in the parameter matrix, covering the width-to -thickness ratios, b/t, from 7 to 41 and depth-to-thickness ratios, d/t, from 6 to 57, as summarized in the Table 5. The member length was chosen case by case to keep the same member

slenderness equal to L_f / r =23 which is also the average of test specimens, with r is the radius of gyration and L is the flexural length.

The input material parameters were defined based on the average of coupon test results. Other assumptions, including the boundary conditions and geometric imperfections, are identical to those considered in the previous section.

A total of 33 models were generated to assess, in conjunction with the test results (n^o=12) , deformation capacity of cold-formed hollow sections with subsequent heat-treatment. Fig.16 shows the total values of parameters *b/t* and *d/t* used for rotation capacity assessment.

5. Rotation Capacity Assessment

5.1 Evaluation of rotation capacity

Parametric study results were analysed in terms of moment and rotation capacity. Compared with the test specimens, the FE models has shown similar trend as regards as the over-strength factor , M_{max}/M_{pl}, and ultimate rotation, Θ_u, as given in Fig. 17 and Fig. 18, respectively.

It can be observed that, moment and rotation capacity tend to decrease with the increase of local slenderness, in particular, moment capacity, $M_{max}/M_{pl,}$ is more affected by width-to-thickness ratio, *b/t*. Whereas, the ultimate rotation level strictly depends on the web-flange interaction. This can be explained because Θ_u is evidently compromised with the developing of local buckling.

Parametric study results are summarized in **Table 6**. In general, rotation capacity values, *R*, are fairly satisfactory in relation to the current cross-section classification. Several cases which are classified as class 2/ Non-Compact can also achieve a rotation capacity level greater than 3 before the onset of local buckling, finding the current limits of both EC3 and AISC360-16 to be rather conservative. This improvement in ductility might be related to the improvement in

steel ductility owing to the heat-treatment. On the other hand, some rectangular sections classified as class1/compact achieved lower plastic deformation than expected.

These findings suggest reviewing the cross-section limits considering the web-flange local buckling interaction.

5.2 Proposed design provisions

With the aim to assessing the influence of width-to-thickness, *b/t*, and depth-to-thickness, *d/t*, on rotation capacity *R*, multiple linear regression analyses were carried out. Relationship between rotational capacity *R* with respect to the *b/t* (a) and in *d/t* (b) ratios are presented in Fig. 19.

Linear regression equations accounting both experimental and numerical results have been derived to find the new width-to-thickness, *b/t* (Eq. 4), and depth-to-thickness, *d/t* (Eq. 5), limits to ensure rotation capacity equal to or greater than 3 and to use cold-formed sections with moderate heat-treatment in plastic design.

$$R = -0.1277 \times \left(\frac{b}{t}\right) + 7.4652 \quad \rightarrow \quad \frac{b}{t} \leq 35 \quad \text{for } 7 \leq \frac{b}{t} \leq 35 \tag{4}$$

$$R = -0.1014 \times \left(\frac{d}{t}\right) + 8.0519 \quad \rightarrow \quad \frac{d}{t} \leq 49 \quad \text{for } 6.2 \leq \frac{d}{t} \leq 57 \tag{5}$$

It is worth mentioning that these design equations are based on the experimental steel strength, specific manufacturing process, experimental setup, assumptions of parameters considered in this study, therefore, caution shall be taken when using the equations for cases beyond the current range of parameters. However, the main purpose of this paper is to investigate effect of flange-web interaction on the flexural behaviour of cold-formed steel hollow sections moderately heat-treated by assessing the rotation capacity R, as detailed in Fig. 20.

6 Conclusions

331 The flexural behaviour of cold-formed steel square and rectangular hollow sections with
332 subsequent moderate heat-treatment has been discussed. A total of 12 beam specimens were
333 tested in three-point simply-supported beams configuration under monotonic loading, covering
334 a variety of section slenderness. Width-to-thickness, *b/t*, and depth-to-thickness, *d/t*, were
335 chosen as key parameters influencing the rotation capacity. The effect of member slenderness
336 was also investigated. Failure modes, moment-rotation response and strain analysis provided
337 indications about the inception of local buckling and the plastic hinge length. A numerical
338 study was subsequently conducted, providing further information on the moment and rotation
339 capacity of the specimens. Once the numerical modelling approach was validated with the
340 experimental results, a more comprehensive parametric study was carried out. The findings
341 provide basis for new cross-section limits for beam members to be used for plastic design. The
342 main conclusions are summarized as follows:

343 1. The comparison of flat and corner coupons results indicate that the final heat treatment
344 actually reduced the cold-work effect with an improvement of ductility in most of the
345 sections, but still present in the corner regions leading to non-homogenous properties.
346 2. On average, yield strength, $f_{y,}$ from corner coupons is 1.15-1.16 higher than yield strength
347 from flat coupons.
348 3. The typical failure mode is local buckling, higher is the section slenderness greater is the
349 dimension of the bulges.
350 4. Most of the specimens are classified as class 1 according to Eurocode 3 and as compact
351 section according to AISC 360-16 and, indeed, they easily achieved high rotation level.
352 Yet, rectangular sections showed lower performance compared to the square sections with
353 similar b/t ratio. Therefore, results suggest reconsidering the web-flange buckling
354 interactions in the flexural behaviour.

5. The cross-section limits provided by the current design codes seem not to be suitable for cold-formed section with subsequent heat-treatment.
6. Experimental and numerical results showed similar trend in terms of moment and rotation capacities. Therefore, they could provide the basis for new cross-section classification accounting the web-flange interaction and the improvement of ductility owing to the final heat-treatment.
7. In general, the results suggest the possibility to relax the width-to-thickness ratio, b/t, and to tighten the depth-to-thickness, d/t, limits.

Acknowledgement

The authors sincerely acknowledge the support received from the Chinese National Engineering Research Centre for Steel Construction (Hong Kong Branch) at The Hong Kong Polytechnic University.

References

[1] BS-EN-10219-1. Cold formed welded structural hollow sections of non-alloy and fine grain steels- Part 1: Technical delivery requirements. *British Standards Institution, London, UK,* 2019.

[2] BS-EN-10219-2. Cold formed welded steel structural hollow sections-Part 2: Tolerances, dimensions and sectional properties. *British Standards Institution, London, UK*, 2019.

[3] BS-EN-10210-1. Hot finished structural hollow sections of non-alloy and fine grain steels.- Part 1: Technical delivery conditions. *British Standards Institution, London, UK* , 2006.

[4] BS-EN-10210-2. Hot finished structural hollow sections of non-alloy and fine grain steels - Part 2: Tolerances, dimensions and sectional properties. *British Standards Institution, London, UK* , 2019.

[5] Zhang, X.-Z., Liu, S., Zhao, M.-S., and Chiew, S.-P. Comparative experimental study of hot formed, hot-finished and cold-formed rectangular hollow sections. *Case Studies in Structural Engineering*, 6:115–129, 2016.

[6] Dwyer, T. J. and Galambos, T. Plastic behaviour of tubular beams columns. *Journal of the Structural Division*, 91(4):153–168; 1965.

[7] Ballio, G. and Calado, L. Steel bent sections under cyclic loads. Experimental and numerical approaches. *Costruzioni metalliche*, 1:97–114; 1986.

[8] Gardner, L., Saari, N., and Wang, F. Comparative experimental study of hot-rolled and cold-formed rectangular hollow sections. *Thin-Walled Structures*, 48(7):495– 507; 2010.

[9] D'Aniello M., L. R. and V., P. Ultimate behaviour of steel beams under non uniform bending. *Journal of Constructional Steel Research*, 78:144–158, 2012.

[10] Foster, ASJ. Gardner, L. and Wang, Y. Practical strain-hardening material properties for use in deformation-based structural steel design. *Thin-walled structures*, 92:115–129; 2015.

[11] Yun, X. and Gardner, L. Stress-strain curves for hot-rolled steels. *Journal of Constructional Steel Research*, 133:36–46; 2017.

[12] Yun, X. and Gardner, L. Numerical modelling and design of hot-rolled and cold-formed steel continuous beams with tubular cross-sections. *Thin-Walled Structures*, 132:574–584; 2018.

[13] Gardner, L. and Yun, X. Description of stress-strain curves for cold-formed steels. *Construction and Building Materials*, 189:527–538; 2018.

[14] EN 1993-1-1: Eurocode 3: Design of steel structures - Part 1-1: General rules and rules for buildings; 2005.

[15] AISC 360-16. Specification for Structural Steel Buildings; 2016.

[16] Bruneau, Michel Eng, P., Uang, C.-M., and Rafael, S. *Ductile design of steel structures*. McGraw-Hill Education; 2011.

405 [17] ISO 6892-1. Metallic Materials—tensile testing—part 1. *International Organization for*
406 *Standardization Geneva, Switzerland;* 2016.
407 [18] Chen, J. and Chan, T.M. Experimental assessment of the flexural behaviour of concrete-
408 filled steel tubular beams with octagonal sections. *Engineering Structures*, 199:109604; 2019.
409 [19] ABAQUS. CAE Simulia 6.13. *Computer software; 2013*.

Table 1. Section properties and classification.

nº	Section	D	B	t_f	t_w	r_o	r_i	b/t	d/t	EC3	AISC360-16
		mm	mm	mm	mm	mm	mm			Class	
1	SHS−100×100×8	100.4	99.8	7.8	7.9	11.7	7.8	10	10	1	Compact
2	SHS−100×100×6.3	100.3	99.5	5.9	6.1	8.8	5.9	14	14	1	Compact
3	SHS−120×120×6.3	120.1	120.1	6.1	6.3	9.1	6.1	17	17	1	Compact
4	SHS−100×100×4	99.3	99.6	3.8	3.7	5.7	3.8	23	23	1	Compact
5	SHS−150×150×5	150.3	150.9	4.9	4.9	7.3	4.9	28	28	2	Non-Compact
6	RHS−120×80×8	119.2	79.7	8	8.1	12.0	8.1	7	12	1	Compact
7	RHS−160×80×6.3	160.8	80.2	6.1	6.2	9.1	6.1	10	23	1	Compact
8	RHS−160×80×5	159.3	79.9	5.1	5	7.5	5	13	29	1	Compact
9	RHS−200×100×5	199.5	100.6	4.9	5.1	7.3	4.9	17	36	1	Compact
10	RHS−250×150×6.3	249.3	149.1	6.2	6.3	9.3	6.2	21	37	1	Compact

Table 2**.** Average material properties*.*

Flat	f_y	E_s	ε_y	ε_{sh}	f_u	ε_u	ε_f	f_u/f_y
	MPa	GPa	%	%	MPa	%	%	
SHS−100×100×8	496.9	204.6	0.24	1.55	562.6	8.23	25.89	1.13
SHS−100×100×6.3	451.1	194.3	0.23	0.97	528	11.61	25.14	1.17
SHS−120×120×6.3	441.1	210.8	0.21	1.72	522.4	11.96	26.24	1.18
SHS−100×100×4	453.7	200.2	0.23	1.46	539.8	10.3	24.23	1.19
SHS−150×150×5	432.1	205.5	0.21	1.65	517.7	12.79	25.08	1.2
RHS−120×80×8	471.3	204.5	0.23	1.5	546.7	10.19	27.04	1.16
RHS−160×80×6.3	406.3	200.1	0.2	1.8	520.1	14.95	28.99	1.28
RHS−160×80×5	455.6	212	0.22	1.97	544.1	11.96	28.11	1.19
RHS−200×100×5	433.5	206.6	0.21	1.67	590.6	14.35	29.05	1.36
RHS−250×150×6.3	427.6	206.2	0.21	1.83	570.9	15.51	26.36	1.34
Mean Value	**446.9**	**204.4**	**0.21**	**1.6**	**544.2**	**12.18**	**26.61**	**1.22**
CoV	0.017	0.008	0.018	0.051	0.013	0.056	0.019	0.019
Corner								
SHS−100×100×8	539.0	194.4	0.28	/	577.5	4.11	14.02	1.07
SHS−120×120×6.3	480.3	195.8	0.24	/	522.5	4.36	16.12	1.08
SHS−100×100×4	528.4	184.4	0.18	/	584.9	4.08	12.45	1.1
Mean Value	**515.9**	**191.5**	**0.23**	**/**	**561.6**	**4.18**	**14.19**	**1.08**
CoV	0.029	0.015	0.102		0.029	0.017	0.061	0.007

Table 3. Test results

n°	Specimens	L_f	M_{pl}	Θ_y	M_{max}	M_u	Θ_u	$\frac{M_{max}}{M_{pl}}$	R
		mm	kNm	rad	kNm	kNm	rad		
1	SHS-100×100×8	875	48.16	0.017	63.31	50.64	/	1.31	>7
2	SHS-100×100×6.3	875	34.87	0.016	51.32	41.06	/	1.47	>7
3	SHS-120×120×6.3	975	51.90	0.014	69.57	55.65	/	1.34	>7
4	SHS-100×100×4 - ST	475	23.09	0.008	26.60	21.28	0.100	1.15	>7
5	SHS-100×100×4 - SL	1275	23.09	0.023	25.81	20.65	0.120	1.12	4.3
6	SHS-150×150×5	1175	66.48	0.013	65.92	52.73	0.062	1.00	3.8
7	RHS-120×80×8	1075	51.67	0.018	76.65	61.32	/	1.48	>7
8	RHS-160×80×6.3	1275	57.20	0.014	75.61	60.49	/	1.32	>7
9	RHS-160×80×5 -ST	1075	52.05	0.012	61.92	49.54	/	1.19	>7
10	RHS-160×80×5 - SL	1875	52.05	0.021	56.62	45.30	/	1.09	>7
11	RHS-200×100×5	1475	81.46	0.013	85.18	68.15	0.056	1.05	3.4
12	RHS-250×150×6.3	2575	169.41	0.017	163.38	130.71	0.045	0.96	1.6

Table 4. Comparison of $\frac{M_{max,FE}}{M_{max,exp}}$ for different assignment conditions of corner and flat material properties.

Specimen	No Corners			Only Corner Region			Corner Region +2t		
	s/100	s/200	s/300	s/100	s/200	s/300	s/100	s/200	s/300
SHS-100×100×8	0.89	0.91	0.98	0.99	1.03	1.05	1.10	1.12	1.13
SHS-120×120×6.3	0.88	0.91	0.96	0.99	1.02	1.07	1.09	1.13	1.17
SHS-100×100×4-ST	0.84	0.86	0.95	0.94	0.98	1.05	1.03	1.10	1.14
SHS-100×100×4-SL	0.82	0.85	0.90	0.93	1.01	1.00	1.04	1.06	1.10
Mean Value	0.86	0.88	0.95	0.96	**1.00**	1.04	1.07	1.10	1.13
CoV	0.017	0.016	0.016	0.014	0.011	0.012	0.014	0.012	0.011

Table 5. Range of b/t and d/t used for parametric study.

Parameters	Minimum	Maximum
Width-to-Thickness ratio, *b/t*	7.0	41.2
Depth-to-Thickness ratio, *d/t*	6.2	57

Table 6. Summary of FE results.

	Section Properties				Parameters		Flexural Performance						Classification
n°	D	B	t_f	L	b/t	d/t	M_{pl}	Θ_y	M_{max}	M_u	Θ_u	R	EC3/AISC360-16
	mm	mm	mm	mm									
1	150	110	4	1311	25	35	46	0.0152	55	44	0.0759	4	1/Compact
2	110	40	4	856	7	25	16	0.0148	22	18	0.1184	7	1/Compact
3	150	50	4	1171	10	35	30	0.0148	43	34	0.1079	6.3	1/Compact
4	200	50	4	1520	10	47	50	0.0147	67	53	0.0588	3.0	1/Compact
5	220	55	4	1677	11	52	60	0.0147	82	66	0.0544	2.7	2/NonCompact
6	280	60	6	2083	7	44	138	0.0147	199	159	0.0762	4.2	1/Compact
7	250	100	6	2017	15	42	128	0.0149	149	119	0.0862	4.8	1/Compact
8	150	110	5	1301	19	27	56	0.0152	61	49	0.0896	4.9	1/Compact
9	190	110	5	1607	19	35	80	0.0150	86	69	0.1128	6.5	1/Compact
10	220	100	4	1817	22	52	78	0.0149	90	72	0.0672	3.5	1/Compact
11	300	100	6	2367	14	47	187	0.0148	228	182	0.1006	5.8	1/Compact
12	60	150	7	555	20	6	26	0.0160	25	20	0.0942	4.9	1/Compact
13	90	150	6	836	22	12	41	0.0157	51	36	0.1100	6	1/Compact
14	140	140	6	1253	20	20	71	0.0154	81	65	0.1123	6.3	1/Compact
15	200	150	6	1747	22	30	123	0.0152	139	111	0.0760	4	1/Compact
16	300	125	6	2441	18	47	207	0.0149	235	188	0.0729	3.9	1/Compact
17	300	150	5	2516	27	57	191	0.0150	179	143	0.0419	1.8	2/NonCompact
18	100	150	10	884	12	7	72	0.0156	90	72	0.1407	8	1/Compact
19	260	180	10	2221	15	23	323	0.0151	385	308	0.1060	6	1/Compact
20	200	150	10	1704	12	17	194	0.0152	263	210	0.1064	6	1/Compact
21	280	160	8	2356	17	32	275	0.0150	325	260	0.0872	4.8	1/Compact
22	280	155	6	2367	23	44	207	0.0150	227	182	0.0676	3.5	1/Compact
23	100	190	10	909	16	7	88	0.0158	110	88	0.1263	7	1/Compact
24	350	150	9	2836	14	36	420	0.0149	520	416	0.0968	5.5	1/Compact
25	330	240	7	2901	31	44	394	0.0152	360	288	0.0531	2.5	2/NonCompact
26	300	180	6	2570	27	47	250	0.0151	258	206	0.0452	2	2/NonCompact
27	180	220	7	1662	28	23	160	0.0155	160	128	0.0714	3.6	1/Compact
28	200	260	9	1848	26	19	262	0.0156	270	216	0.0778	4	1/Compact
29	250	250	7	2277	33	33	274	0.0154	228	182	0.0846	4.5	1/Compact
30	340	280	9	3021	28	35	573	0.0153	541	433	0.0748	3.9	1/Compact
31	200	200	5	1827	37	37	126	0.0154	95	76	0.0585	2.8	2/NonCompact
32	200	200	5	1832	41	41	114	0.0154	82	66	0.0446	1.9	2/NonCompact
33	180	230	6	1681	35	27	143	0.0155	125	100	0.0622	3.0	1/Compact

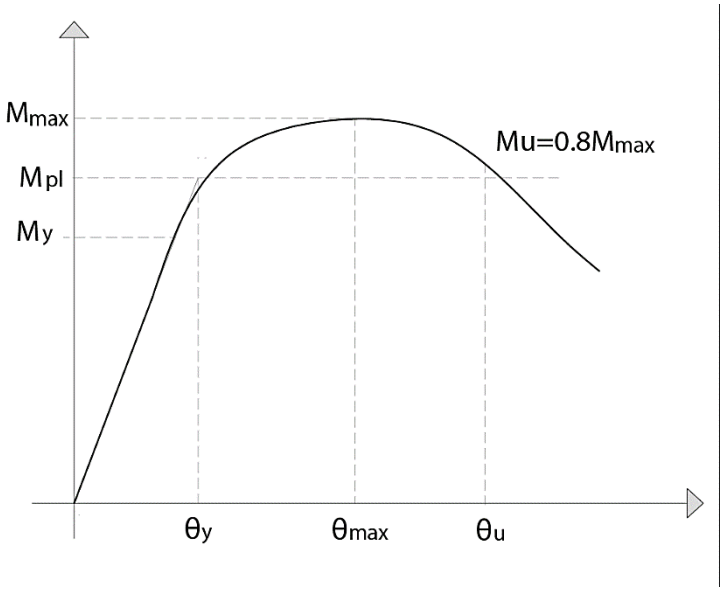

Fig. 1 Generalized moment-rotation curve

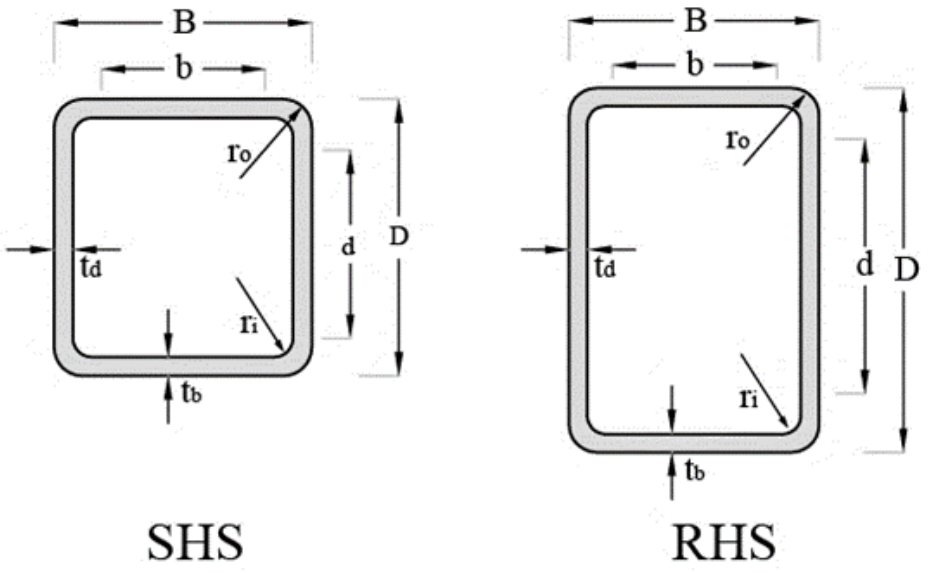

Fig *2*. Square Hollow Section (SHS) and Rectangular Hollow Section (RHS) with geometric symbols

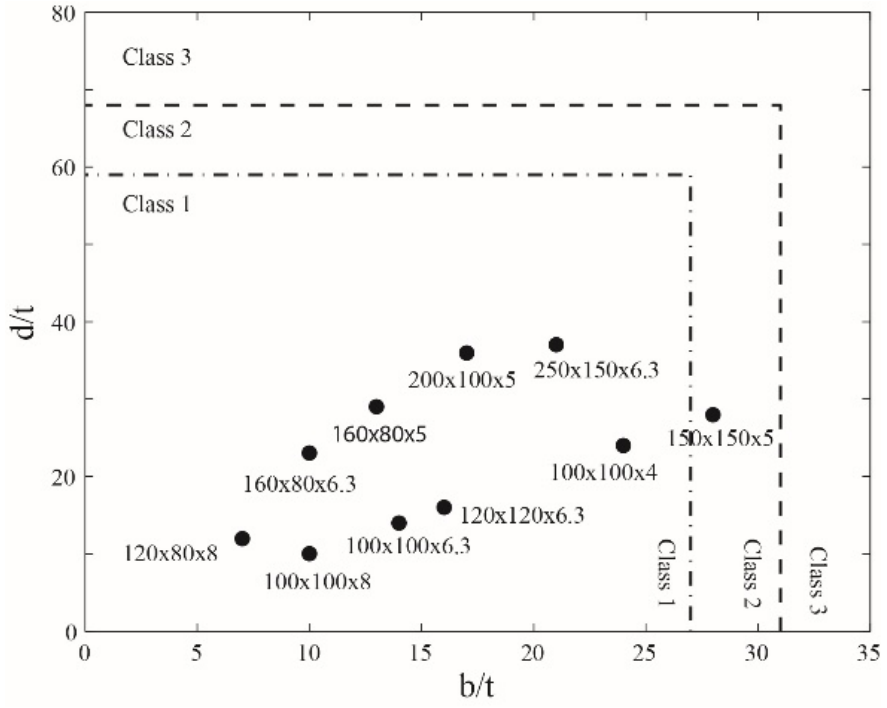

(a) EN 1993-1-1

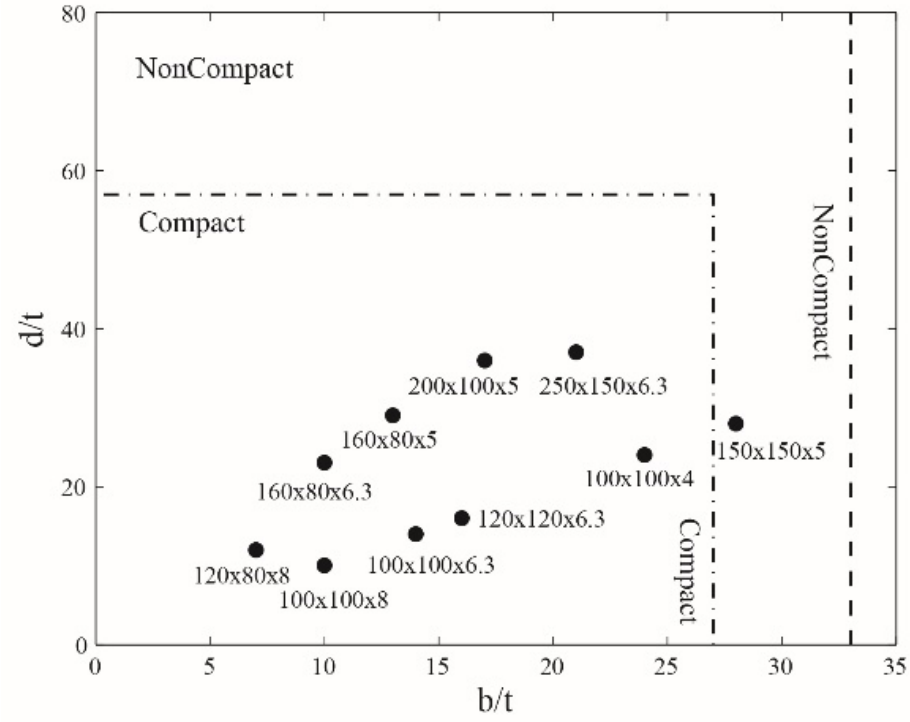

(b) AISC 360-16

Fig. 3 Width-thickness, b/t, and depth-thickness, d/t, ratios of the tested beams compared with limits in (a) EN 1993-1-1 and (b) AISC 360-16.

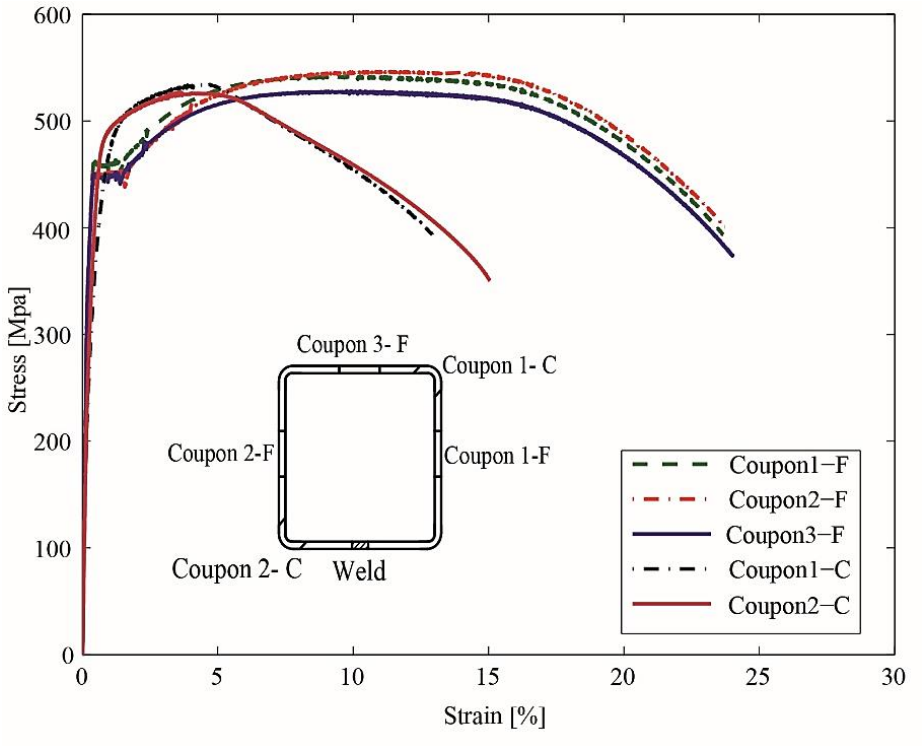

Fig. 4. Typical stress-strain curves results of cold-formed sections with moderate heat-treatment.

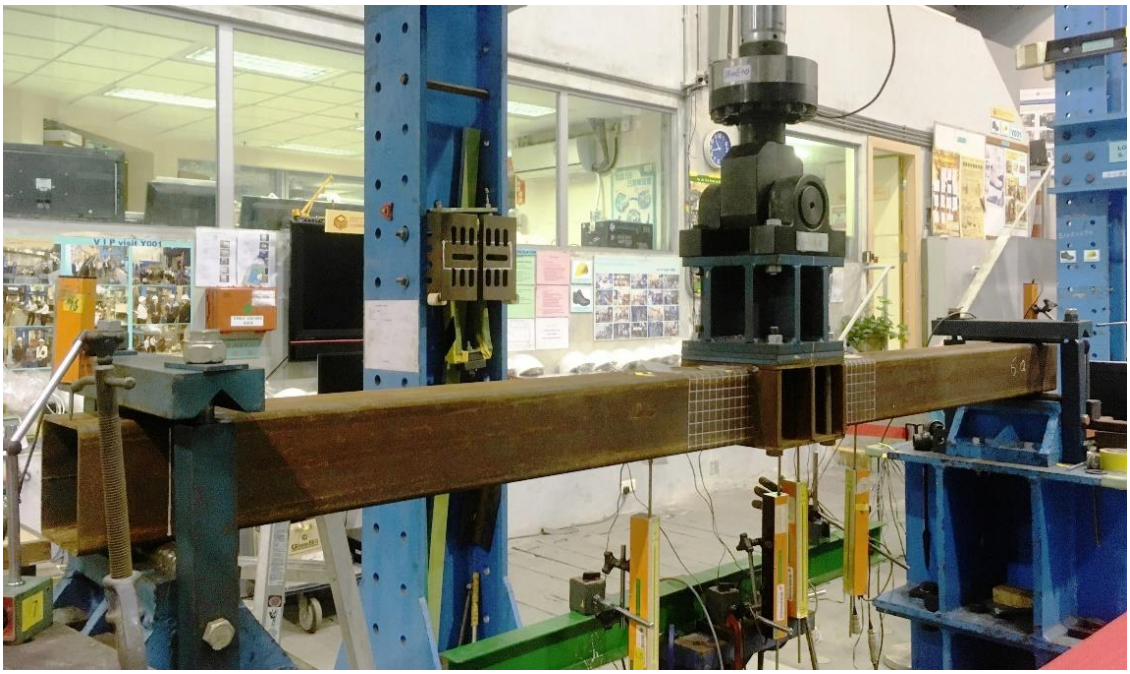

Fig. 5 Experimental test setup of beam test.

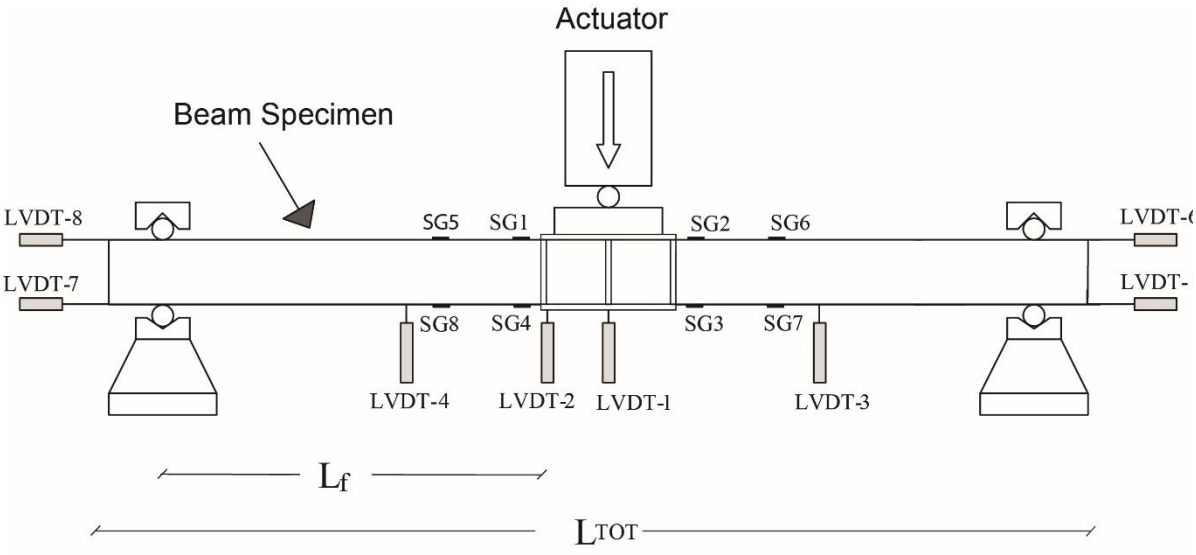

Fig. 6 Schematic test setup and instrumentation.

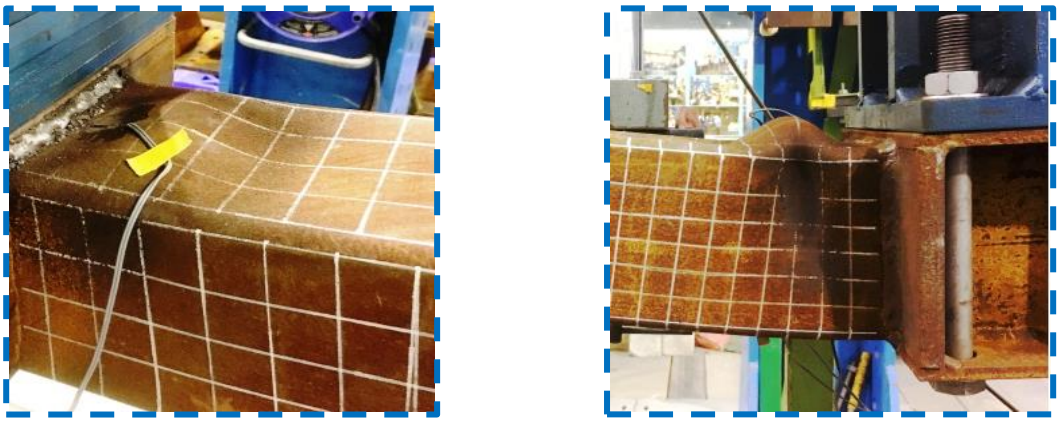

(a) (b)

Fig. 7 Typical failure modes of specimens: (a) flange local buckling and (b) web-flange local buckling.

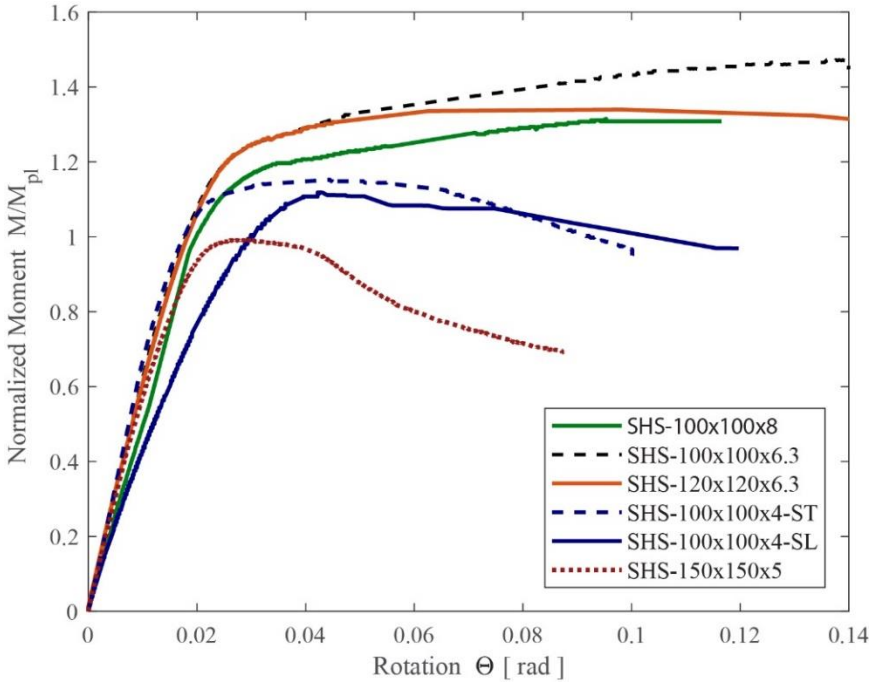

(a) Square hollow sections

(b)

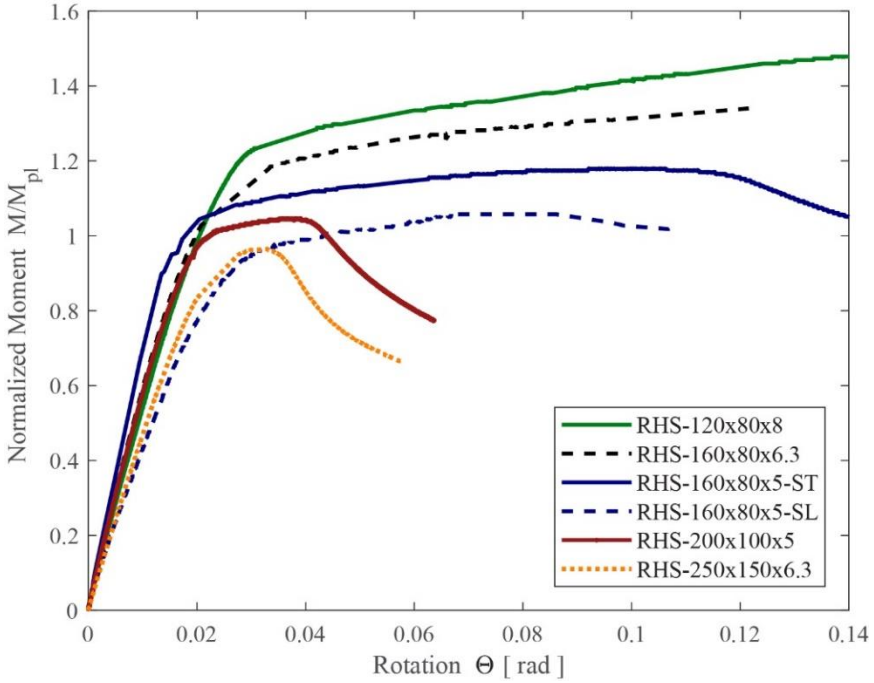

(c) Rectangular hollow sections

Fig.8 Normalized Moment-Rotation curves in (a) Square Hollow Sections (SHSs) and (b) Rectangular Hollow Sections (RHSs).

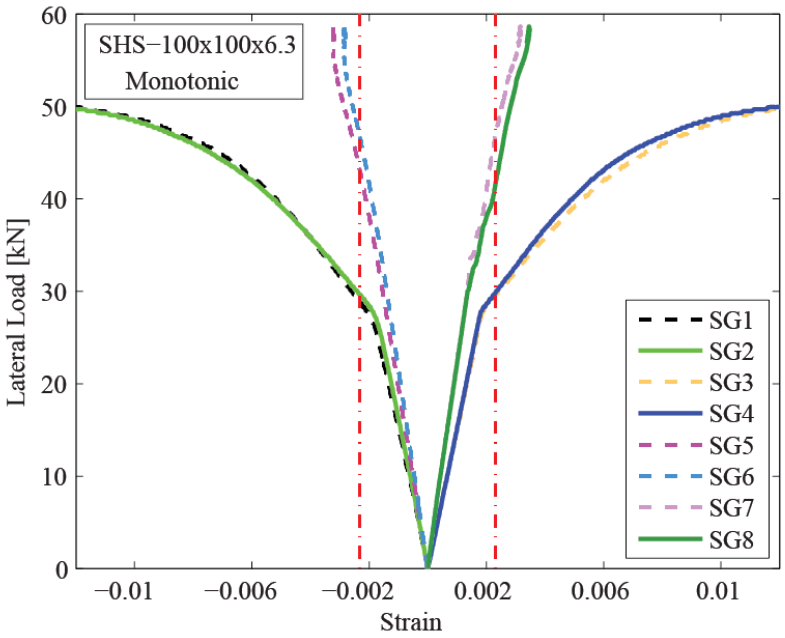

(a) SHS-100 × 100 × 6.3

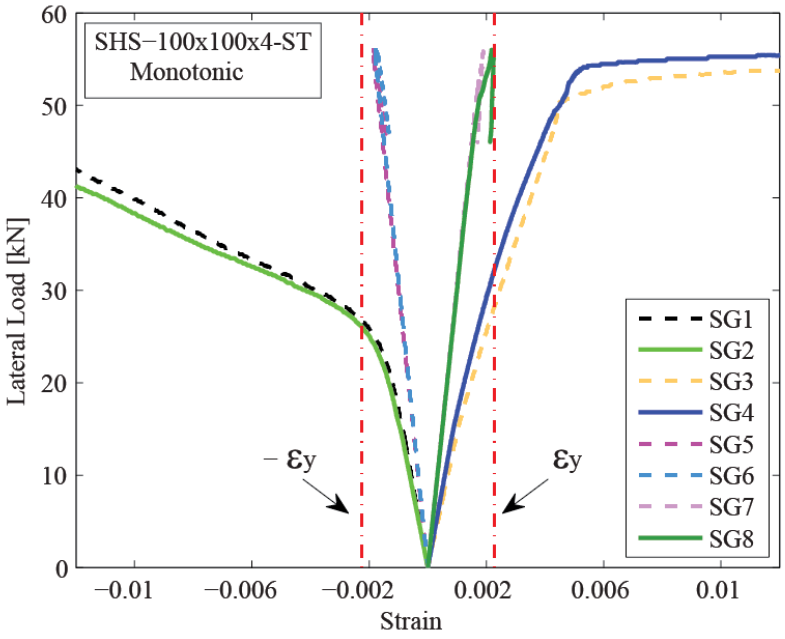

(b) SHS−100 × 100 × 4−ST

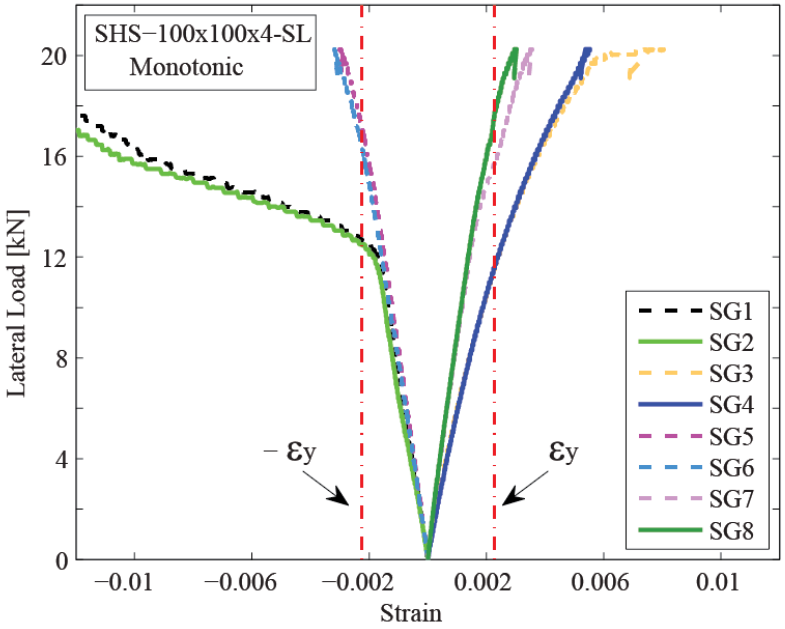

(c) SHS-100 × 100 × 4–SL

Fig.9 Strain analysis: lateral load versus steel strains in (a) SHS-100 × 100 × 6.3, (b) SHS−100 × 100 × 4−ST and (c) SHS-100 × 100 × 4–SL.

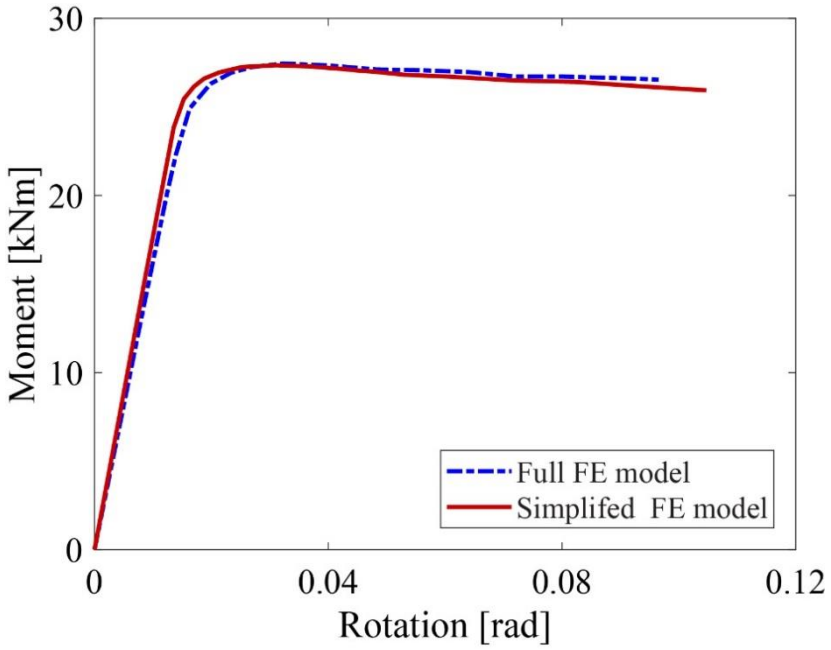

(a) Moment-rotation curves

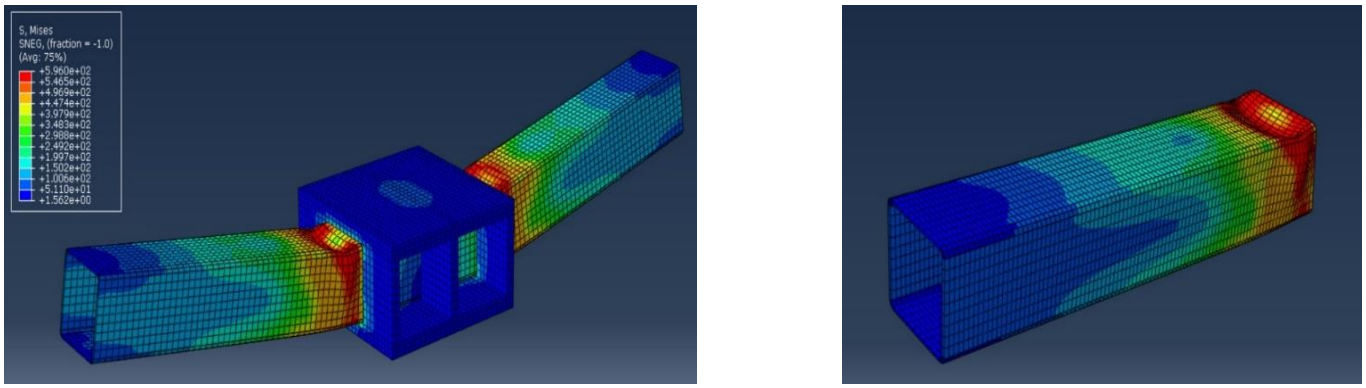

(b) Failure modes

Fig.10 Full versus Simplifed FE models (a) Moment-rotation curves (b) failure modes

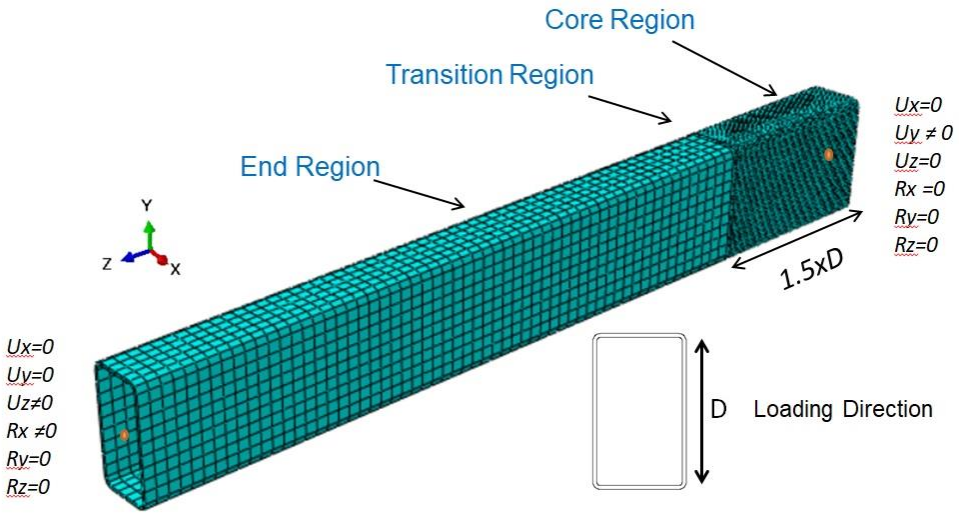

Fig.11 Boundary conditions and mesh discretization of FE model

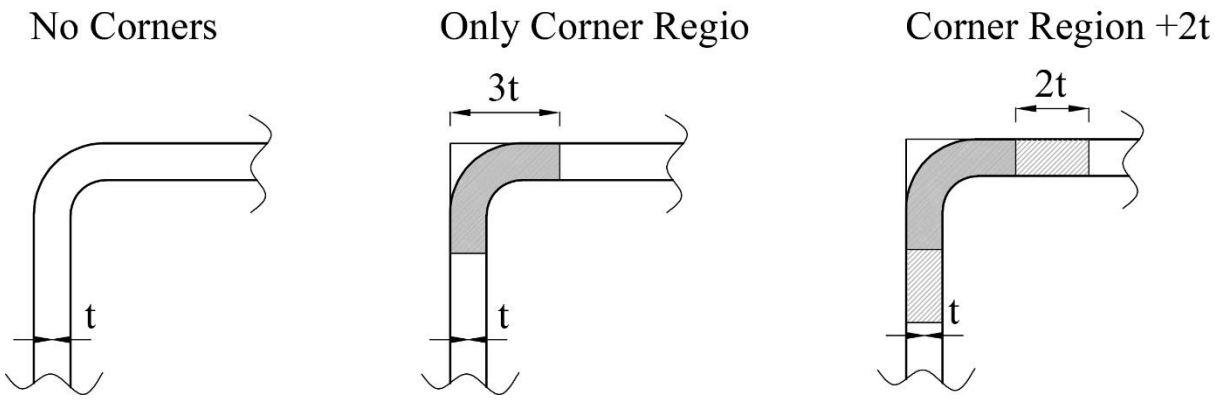

Fig.12 Proposed assignment conditions of corner material properties.

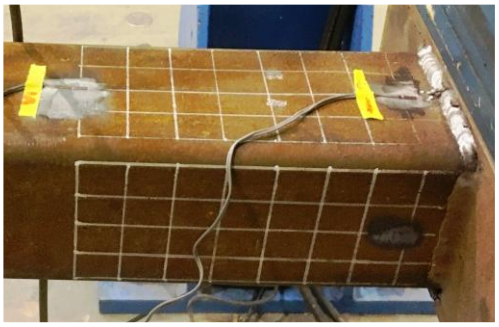

(a.1) Exp, SHS-100×100×6.3

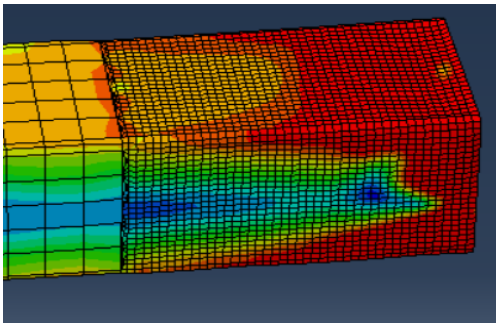

(b.1) FE, SHS-100×100×6.3

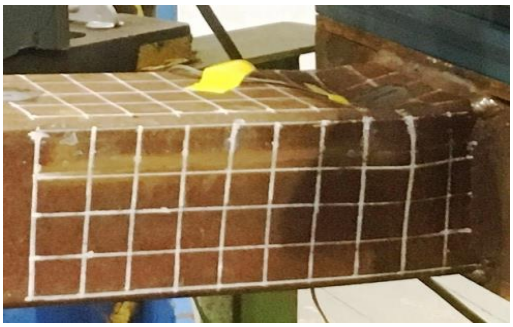

(a.2) Exp, SHS-100×100×4-ST

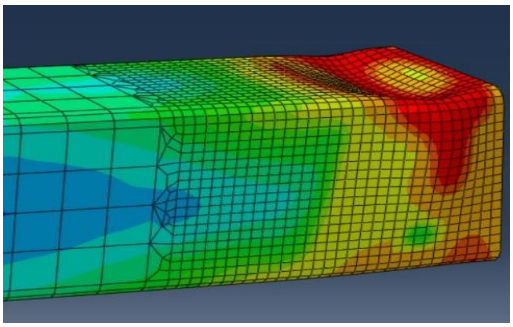

(b.2) FE, SHS-100×100×4-ST

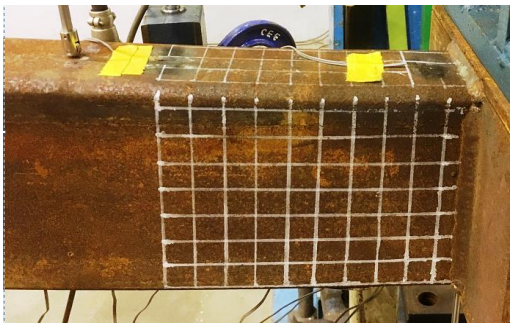

(a.3) Exp, RHS-160×80×6.3

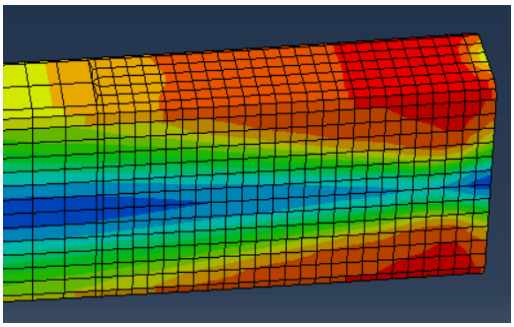

(b.3) FE, RHS-160×80×6.3

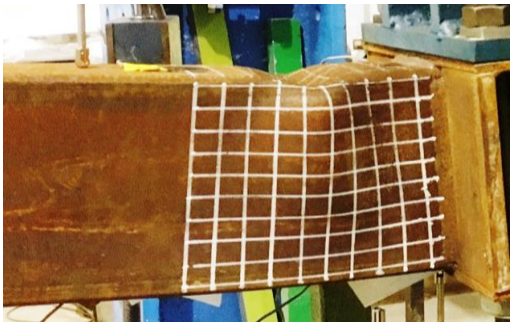

(a.4) Exp, RHS-200×100×5

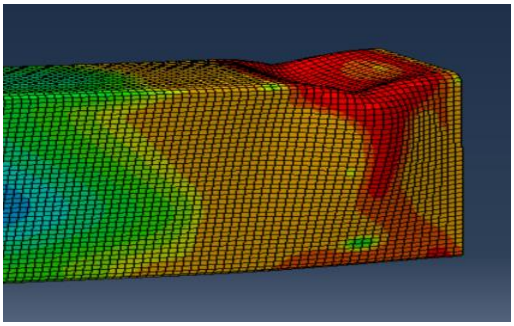

(b.4) FE, RHS-200×100×5

Fig. 13. Typical failure patterns observed in (a) tests and (b) Finite Element FE models

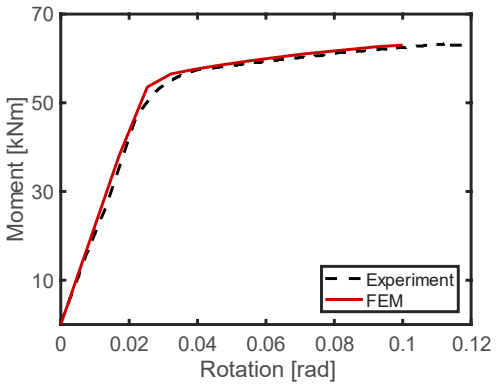

(a) SHS-100×100×8

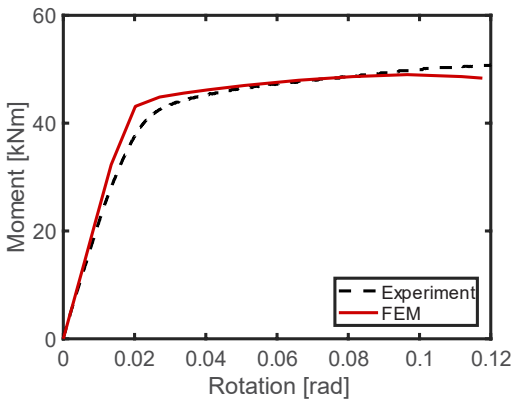

(b) SHS-100×100×6.3

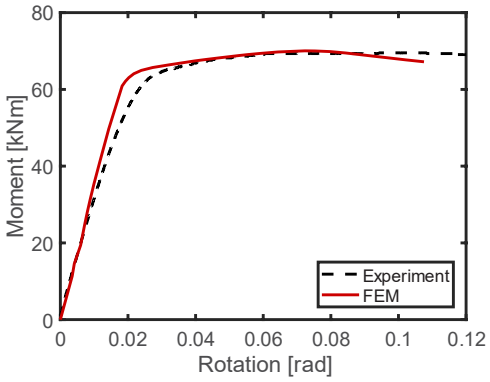

(c) SHS- 120×120×6.3

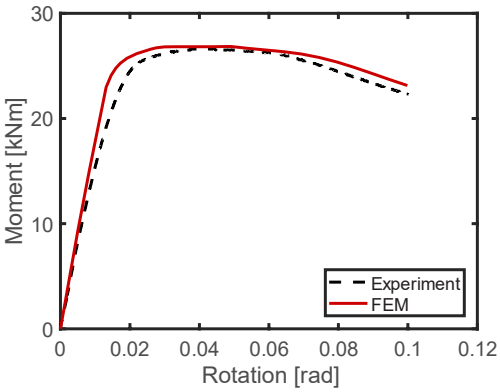

(d) SHS-100×100×4-ST

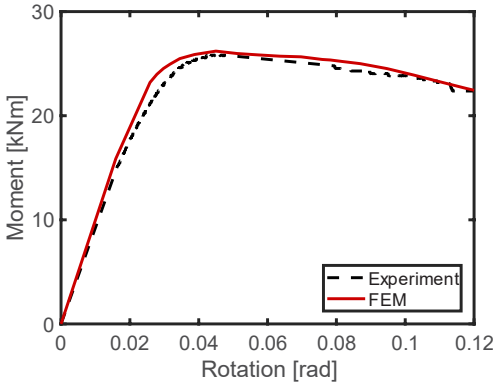

(e) SHS-100×100×4-SL

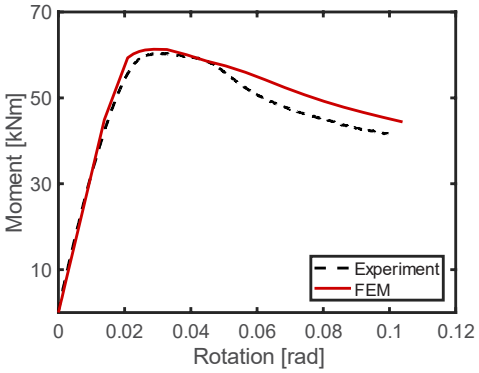

(f) 1 SHS-50×150×5

Fig. 14. SHS-Experimental and FEM simulated moment-rotation curves

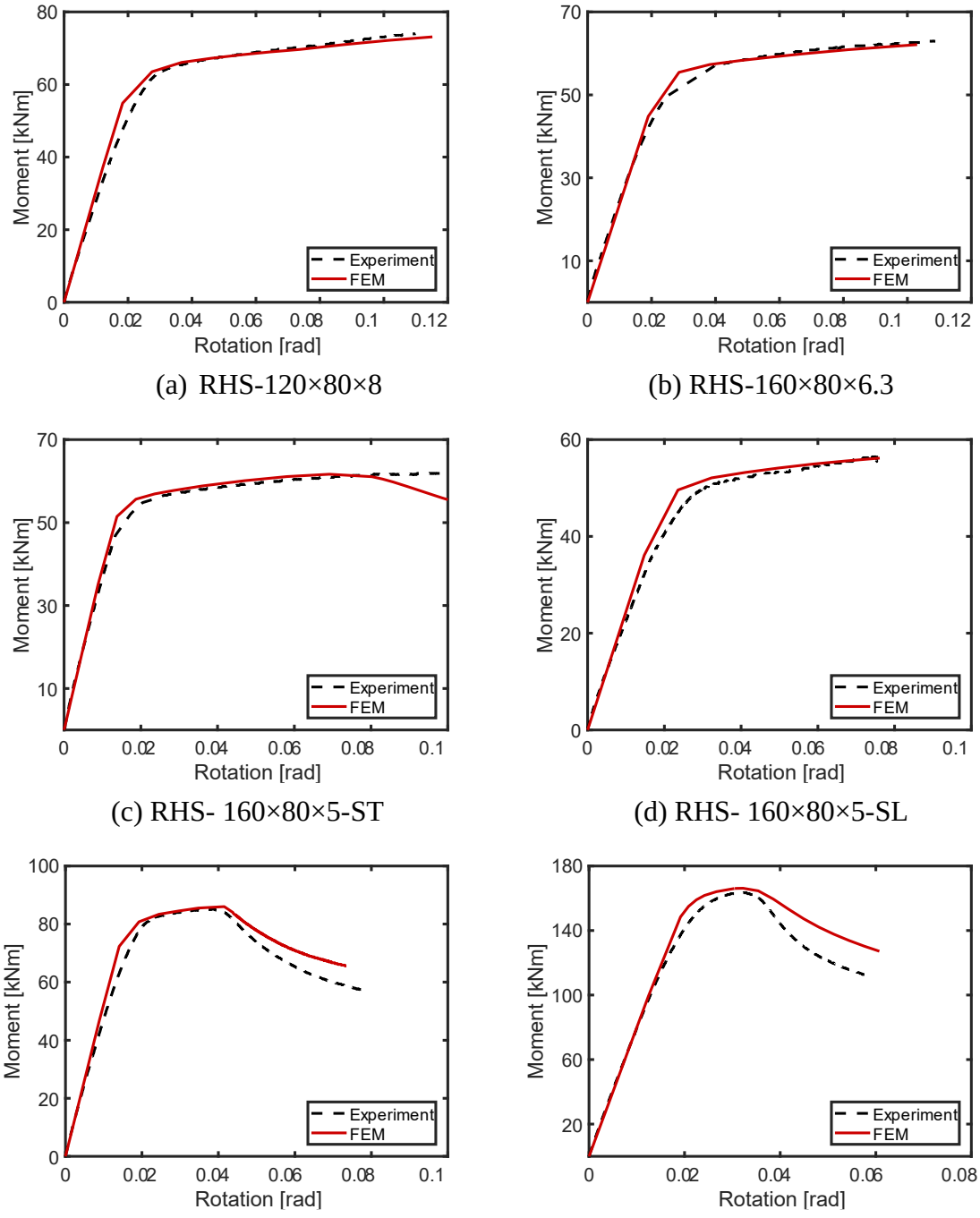

(a) RHS-120×80×8 (b) RHS-160×80×6.3

(c) RHS- 160×80×5-ST (d) RHS- 160×80×5-SL

(e) RHS-200×100×5 (f) RHS-250×150×6.3

Fig. 15. RHS-Experimental and Finite Element simulated moment-rotation curves

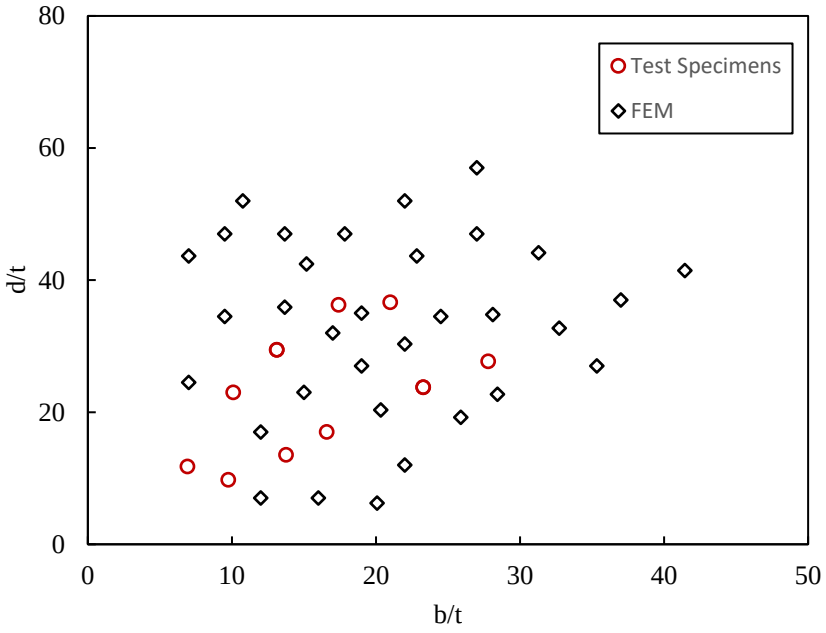

Fig. 16 Values of b/t and d/t used for rotation capacity assessment.

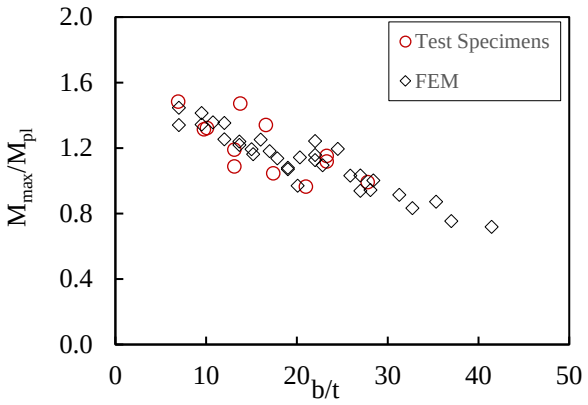

(a) Width-to-thickness ratio

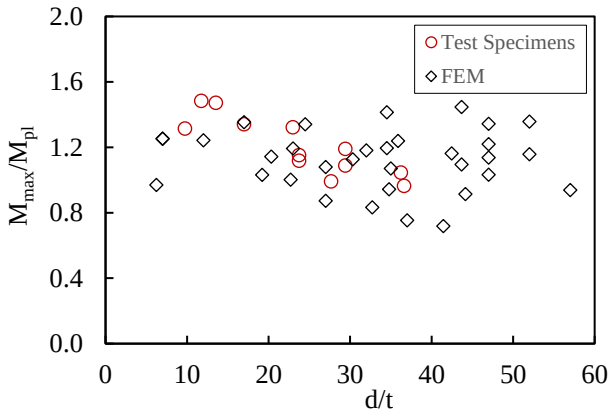

(b) Depth-to-thickness ratio

Fig.17 Moment Capacity against (a) width-to-thickness, b/t, and (b) depth-to-thickness, d/t, ratios

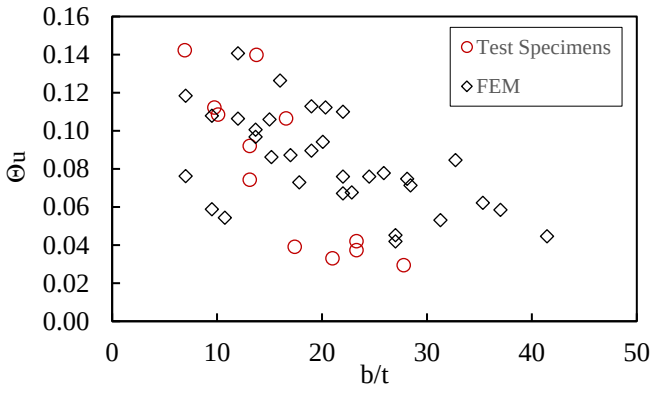

(a) Width-to-thickness

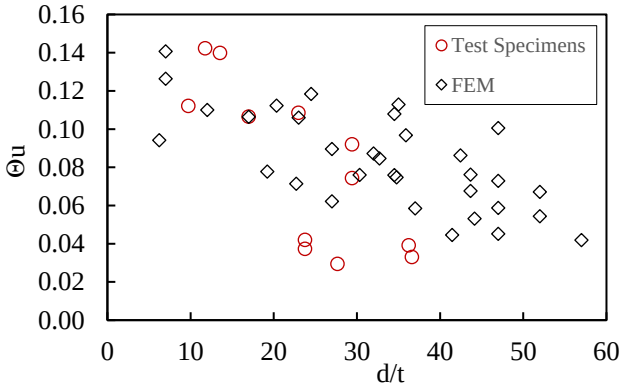

(b) Depth-to-thickness

Fig.18 Ultimate rotation Θu against (a) width-to-thickness, b/t, and (b) depth-to-thickness, d/t, ratios

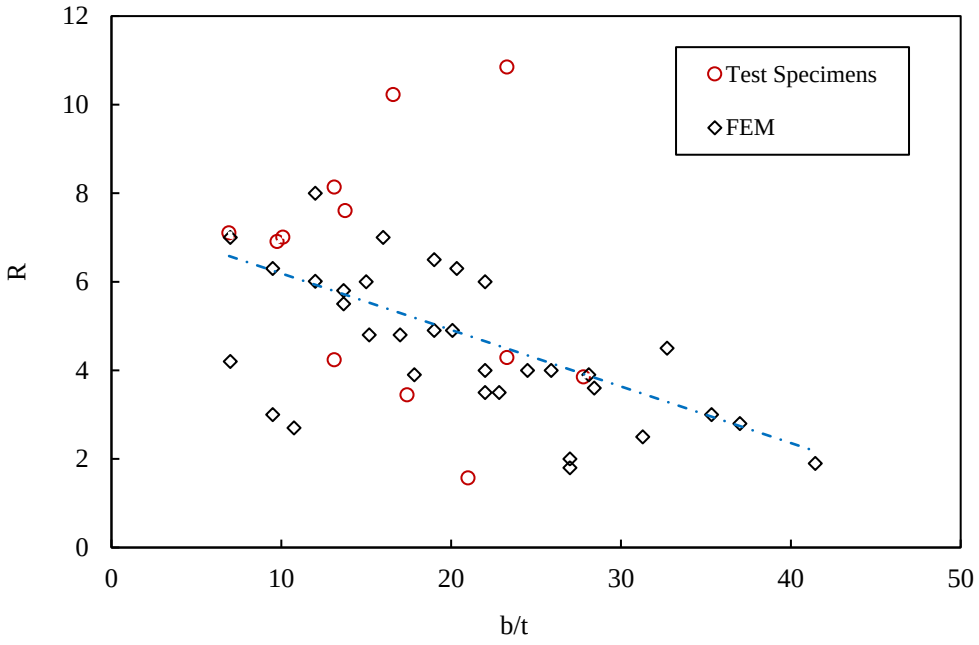

(a) Width-to-thickness ratio

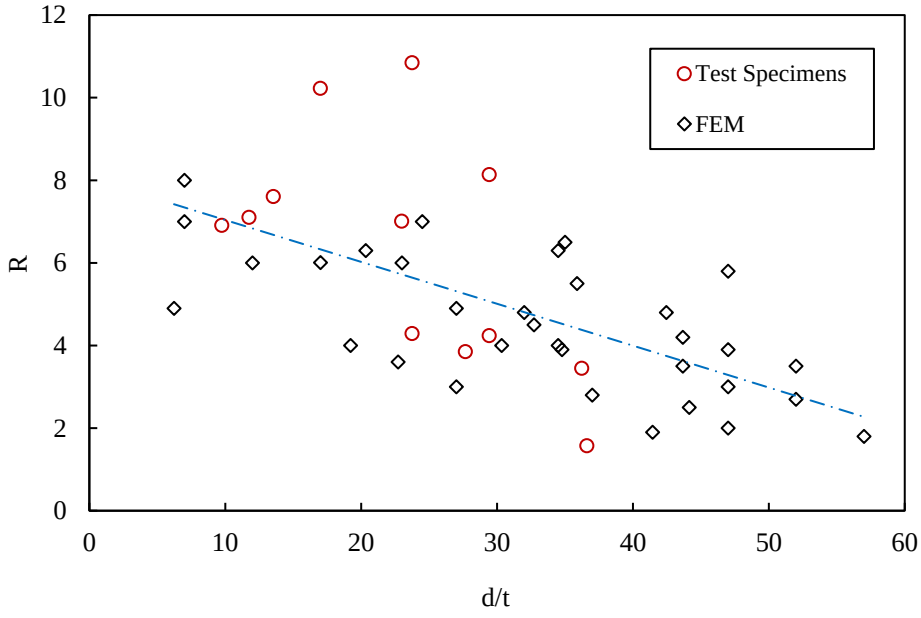

(b) Depth-to-thickness ratio

Fig.19. Effect of the (a) *b/t* and (b) *d/t* ratios on the rotational capacity *R* for test specimens and FEM results.

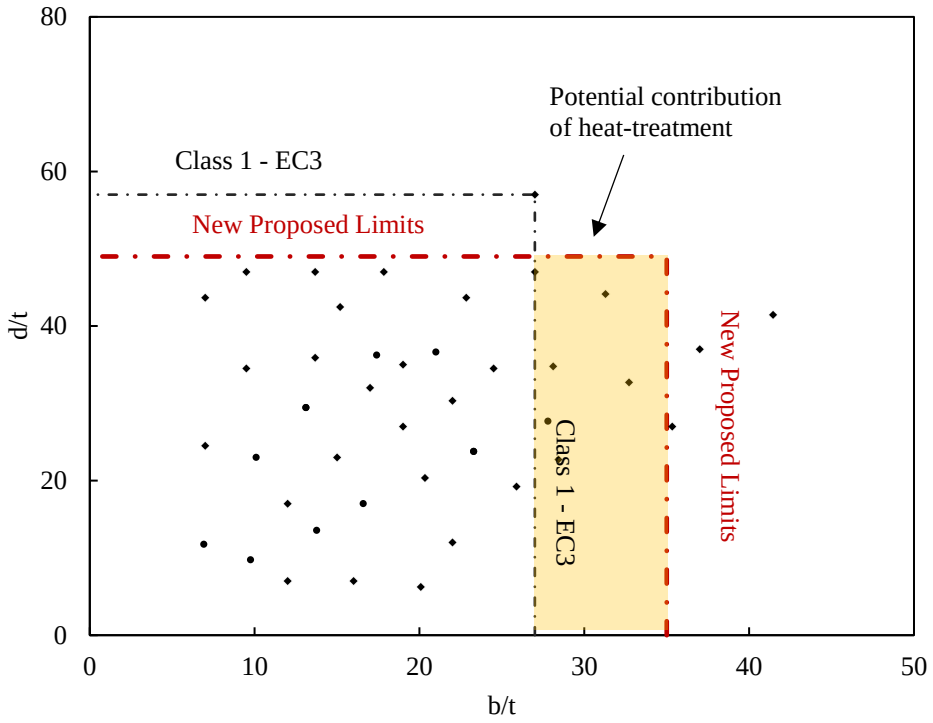

Fig. 20 New proposed limits for plastic design of cold-formed hollow steel section with moderate heat-treatment